J Mater Sci (2011) 46:3523–3536
DOI 10.1007/s10853-011-5262-9

Se and Te-modified titania for photocatalytic applications

Václav Štengl · Snejana Bakardjieva · Jana Bludská

Received: 9 August 2010 / Accepted: 6 January 2011 / Published online: 14 January 2011

Abstract Nanosized Se^{4+} and Te^{4+}, respectively, doped titania was prepared by homogeneous hydrolysis of titanium oxo-sulfate with urea in aqueous solutions in the presence of amorphous selenium and tellurium. The prepared samples were annealing at temperature 200 and 400 °C. The structure of prepared samples was characterized by X-ray powder diffraction (XRD), selected area electron diffraction (SAED), surface area (BET), and porosity determination (BJH). The morphology and microstructure characteristics were obtained by scanning electron microscopy (SEM) and high-resolution electron microscopy (HRTEM). The method of UV/Vis diffuse reflectance spectroscopy was employed to estimate band-gap energies of the Se and Te-doped titania. The photocatalytic activity of the prepared samples was assessed by the photocatalytic decomposition of Orange II dye in an aqueous slurry during irradiation at 365 and 400 nm wavelength. The best photocatalytic activity in UV and visible area exhibit the Se and Te-doped titania samples labeled TiSe3 (~11.5 wt% Se) and TiTe3 (~8.0% Te), respectively.

Introduction

Currently are looking for new photocatalytic TiO_2-based materials that have good activity in the visible light spectrum. One possibility is to replace another metal instead of Ti in the crystal lattice and thus increase the photocatalytic activity. Doping metal ions has disadvantages such as thermal instability and increasing production recombination centers. Another case is the doping of TiO_2 with nonmetal atoms, such as nitrogen [1], sulfur [2], boron [3], iodine [4], or fluorine [5]. In this case the photocatalytic activity depends on the content of nonmetal atoms and the method of preparation. To be able to use synergy effects have been developed co-doped systems, when the titanium dioxide doped multiple elements. These include TiO_2 co-doped nitrogen and fluorine, nitrogen, and sulfur, nitrogen and carbon, or chlorine and bromine. For example, the system doped with nitrogen and fluorine has improved photocatalytic properties that nitrogen improves the absorption of visible light and fluoride can enhance the surface acidity and adsorption of reactants [6]. One of the most overlooked opportunities in the preparation of photocatalytic TiO_2-based materials for visible light is doping with selenium and tellurium.

Sol–gel processing routes have been developed for the production of thin films and powders in the system TeO_2–TiO_2 from tellurium and titanium alkoxides. Pure sol–gel derived TeO_2 thin films are difficult to prepare with good optical transparency due to the presence of organic impurities and/or a highly dispersed metallic tellurium phase when heated at temperatures up to approximately 340 °C, with crystallization to α-TeO_2 occurring when the heat treatment temperature is further increased. Additions of TiO_2 were found to retard the crystallization of the α-TeO_2 but promote the formation of other TiO_2 or $TiTe_3O_8$ phases [7]. The photocatalytic properties of TiO_2 nano-crystals can be enhanced by doping, which can result in increased absorption in the visible range. After annealing Te-modified TiO_2 nano-crystals, the powder becomes photo-sensitive, changing from an off-white color to a dark red color under UV and visible illumination. In TiO_2–Te nanocrystals annealed between 300 and 600 °C, light exposure

V. Štengl (✉) · S. Bakardjieva · J. Bludská
Institute of Inorganic Chemistry AS CR v.v.i.,
250 68 Řež, Czech Republic
e-mail: stengl@iic.cas.cz

quickly causes the visible absorption to increase until the sample is reddish-brown [8]. Anatase TeO_2/TiO_2 nanocomposite was synthesized by a hydrothermal process in the given reaction condition [9]. In the paper [10], aiming to enhance the use of solar energy, SeO_2 was introduced into TiO_2 nanocrystalline and the SeO_2/TiO_2 nanocomposite was prepared by water bathing and calcining using SeO_2 and titanium butoxide as precursors. The photodeposition of cadmium selenide (CdSe) using Se–TiO_2 photocatalysts was studied at pH 3.5 and 7 in the presence of formic acid. The Se–TiO_2 photocatalysts were obtained by Se ion photoreduction using selenite (Se(IV)) and selenate (Se(VI)) as precursors [11].

The aim of the present work was to synthesize Se and Te, respectively, doped nanoparticles with variable Se(Te)/Ti ratio and appropriate microstructure characteristics, allowing its application as a photocatalyst in an aqueous solution. Homogeneous hydrolysis of titanium oxo-sulfate with urea in aqueous solution in the presence of amorphous selenium and tellurium, respectively, has been chosen as a way of synthesis. The obtained precursors were heated at temperature 200 and 400 °C under oxygen atmosphere. The attention has been paid not only to ratio Se(Te)/Ti but also to crystal structure, BET surface area, particle size, porosity, and the effect of the doped titania nanocrystals on the photocatalytic activity. The photocatalytic activity was studied under UV and visible light by measuring of Orange II disappearance. Pure non-doped titania sample was used as a comparing standard. The present work, and it should be emphasized and taken as a fact, deals as first with the preparation of Se and Te-doped titania in aqueous solution.

Experimental

Synthesis of Se and Te-doped titania

All chemical used, titanium oxo-sulfate, urea, selenium, and tellurium powder were of analytical grade and were supplied by Fluka and Sigma–Aldrich Ltd.

The Se and Te-modified titania was prepared by homogenous hydrolysis of titanium oxo-sulfate with urea, so that the TiO_2 is precipitated on Se or Te. These elements are the nucleus for the precipitation of titania. The titanium oxo-sulfate (100 g) was dissolved in 500 mL hot water acidified with 98% H_2SO_4 to pH $\sim$ 1.2. The pellucid liquid was diluted into 4 L of distilled water, added the defined amount of Se or Te (see Table 1) and mixed with 300 g of urea. The mixture was heated to 100 °C under stirring and kept at this temperature for 6 h until pH 7.2–7.5 was reached and ammonia escaped from the solution. The precipitates formed have been washed by distilled water with decantation, filtered off and dried at temperature of 105 °C in drying oven.

In the remainder of this paper, five new Se-doped TiO_2 samples denoted as TiSe_1–TiSe_5 and another five Te-doped TiO_2 samples named as TiTe_1–TiTe_5 were obtained.

The reference sample was also prepared without Se or Te. All as-prepared samples were heated in quartz tube to 200 and 400 °C for 2 h under oxygen atmosphere, using a furnace controlled by the PID controller. The temperature increase rate was 5 °C min^{-1}. After the heat treatment, the sample was allowed to cool to room temperature.

It is worth to mentioned that annealing of as-prepared samples was accompanied by significant changes in color. In case of Se–TiO_2 samples visible change from light to dark orange was registrated after annealing at 200 °C and light yellow color was resulted for over 400 °C. The Te–TiO_2 system established light gray color after annealing at 200 °C corresponded probably to the color of amorphous Te. Dramatic change from light yellow to dark brown color was observed in case of sample named TiTe_5 after annealing after 400 °C.

Characterization methods

Diffraction patterns were collected with diffractometer PANalytical X'Pert PRO equipped with conventional X-ray tube (Cu Kα radiation, 40 kV, 30 mA) Qualitative analysis was performed with the DiffracPlus Eva software package (Bruker AXS, Germany) using the JCPDS PDF-2 database [12]. For quantitative analysis of XRD patterns we used Diffrac-Plus Topas (Bruker AXS, Germany,

Table 1 Experimental conditions, EDX analysis, BET, and pore size distribution TiO_2/Se/Te

Sample	Se (g)	Surface area (m^2 g^{-1})	Total pore volume (cm^3 g^{-1})	Sample	Te (g)	Surface area (m^2 g^{-1})	Total pore volume (cm^3 g^{-1})
TiSe1	1	304.2	0.2248	TiTe1	1	302.1	0.1935
TiSe2	2	286.3	0.2524	TiTe2	2	308.8	0.2490
TiSe3	3	277.7	0.2099	TiTe3	3	277.4	0.2243
TiSe4	5	251.3	0.2265	TiTe4	5	251.8	0.2064
TiSe5	10	234.2	0.1901	TiTe5	10	176.2	0.1442

version 4.1) with structural models based on ICSD database [13].

Transmission electron micrographs (TEM and HRTEM) were obtained using JEOL JEM 3010 microscope operated at 300 kV (LaB6 cathode).

Scanning electron microscopy (SEM) studies were performed using a Philips XL30 CP microscope equipped with energy dispersive X-ray microanalysis (EDAX), Robinson, secondary electron (SE), and back-scattered electron (BSE) detectors.

The surface areas of samples were determined from nitrogen adsorption–desorption isotherms at liquid nitrogen temperature using a Coulter SA3100 instrument with outgas 15 min at 150 °C. The Brunauer–Emmett–Teller

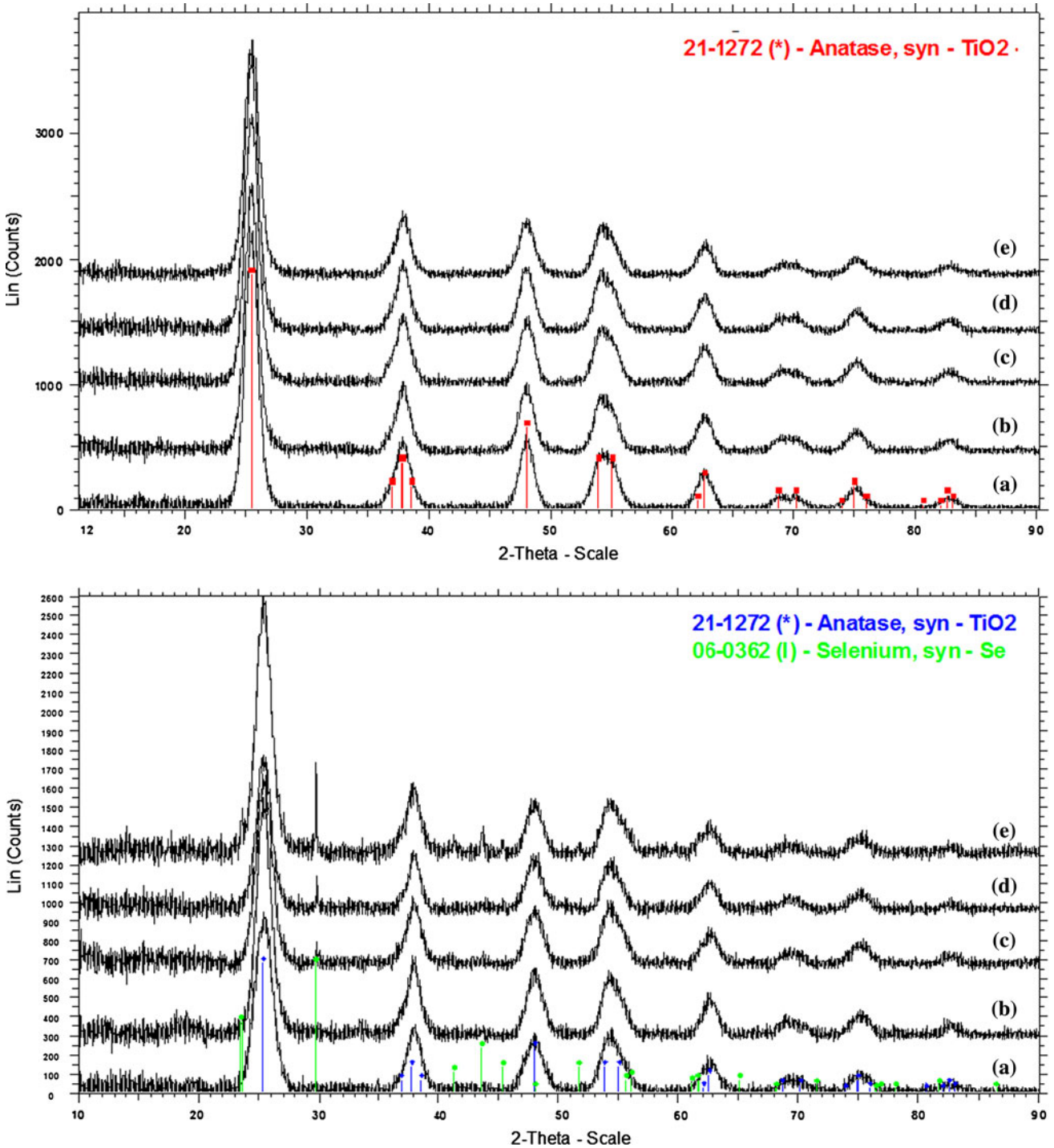

Fig. 1 XRD spectra of Se-doped titania heated at 200 and 400 °C. (*a*) TiSe1, (*b*) TiSe2, (*c*) TiSe3, (*d*) TiSe4, (*e*) TiSe5

(BET) method was used for surface area calculation [14], the pore size distribution was determined by the Barrett–Joyner–Halenda (BJH) method [15].

Diffuse reflectance UV/Vis spectra for evaluation of photophysical properties were recorded in the diffuse reflectance mode (R) and transformed to absorption spectra through the Kubelka–Munk function [16]. A Perkin-Elmer Lambda 35 spectrometer equipped with a Labsphere RSAPE-20 integration sphere with $BaSO_4$ as a standard was used.

Photocatalytic activity of samples was assessed from the kinetics of the photocatalytic degradation of 0.02 M Orange II dye (sodium salt 4-[(2-hydroxy-1-naphtenyl)azo]-benzene-sulfonic acid) in aqueous slurries. The azo-dyes

Table 2 Crystallite size, EDX, BET, and pore size distribution of 400 °C heated samples TiO_2/Se/Te

Sample	Anatase (nm)	Surface area ($m^2\ g^{-1}$)	Total pore volume ($cm^3\ g^{-1}$)	EDX Se (wt%)	Sample	Surface area ($m^2\ g^{-1}$)	Total pore volume ($cm^3\ g^{-1}$)	EDX Te (wt%)
TiSe1_400	15.3	147.7	0.1530	3.19	TiTe1_400	187.7	0.1414	3.1
TiSe2_400	14.9	175.0	0.2038	5.96	TiTe2_400	170.1	0.1801	5.7
TiSe3_400	15.1	180.8	0.2198	9.07	TiTe3_400	157.7	0.1636	8.2
TiSe4_400	15.4	195.3	0.2366	9.41	TiTe4_400	70.2	0.0904	15.3
TiSe5_400	12.4	172.2	0.1900	13.01	TiTe5_400	4.5	0.0186	17.9

Table 3 Phase composition and crystallite size of 200 °C heated samples TiO_2/Se/Te

Sample	Anatase (wt%)	Selenium (wt%)	Anatase (nm)	Sample	Anatase (wt%)	Tellurium (wt%)	Anatase (nm)
TiSe1_200	100	0.05	11.8	TiTe1_200	99.95	0.05	13.5
TiSe2_200	99.94	0.06	12.6	TiTe2_200	99.82	0.18	13.2
TiSe3_200	99.93	0.07	13.1	TiTe3_200	99.74	0.26	13.3
TiSe4_200	99.81	0.19	13.5	TiTe4_200	99.44	0.56	13.6
TiSe5_200	98.85	1.15	13.6	TiTe5_200	98.23	1.77	13.7

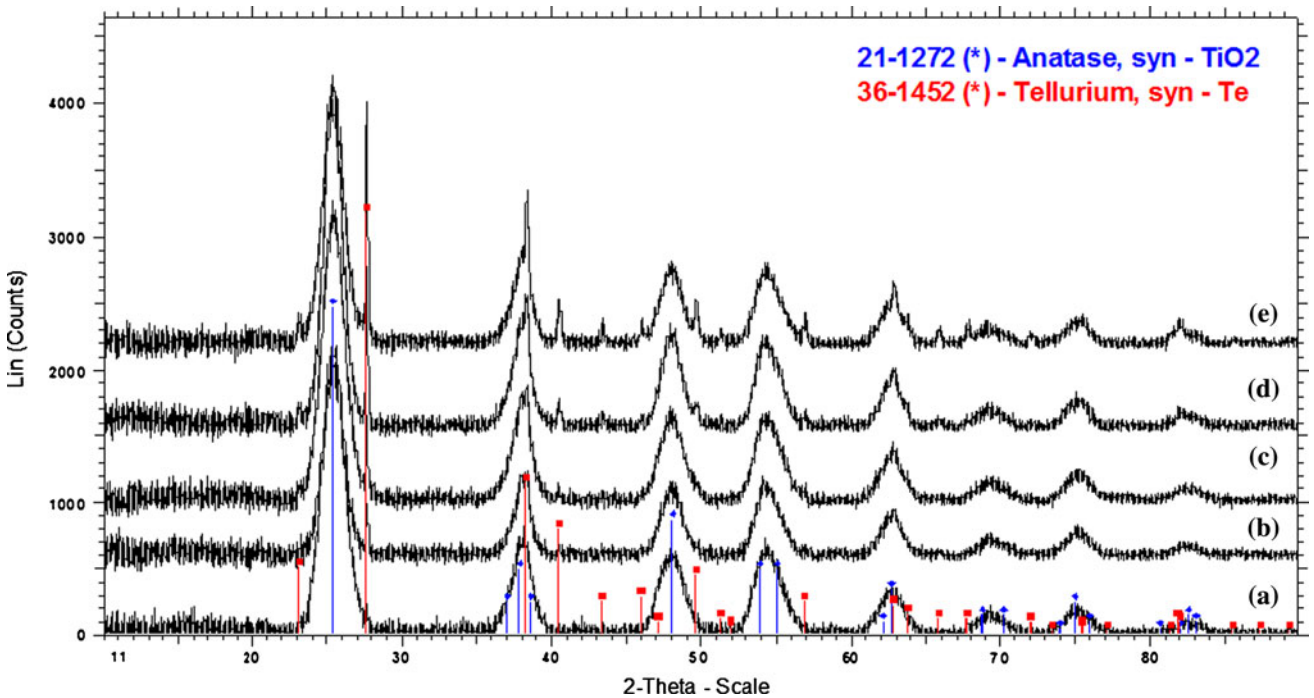

Fig. 2 XRD spectra of Te-doped titania heated at 200 °C. (*a*) TiTe1, (*b*) TiTe2, (*c*) TiTe3, (*d*) TiTe4, (*e*) TiTe5

(Orange II, Methyl Red, Congo Red, etc.) are not absorbed on titania surfaces in contrast to methylene blue. For azo-dye degradation, the complete mass balance in nitrogen indicated that the central –N=N– azo-group was converted in gaseous dinitrogen, which is ideal for the elimination of nitrogen-containing pollutants, not only for environmental

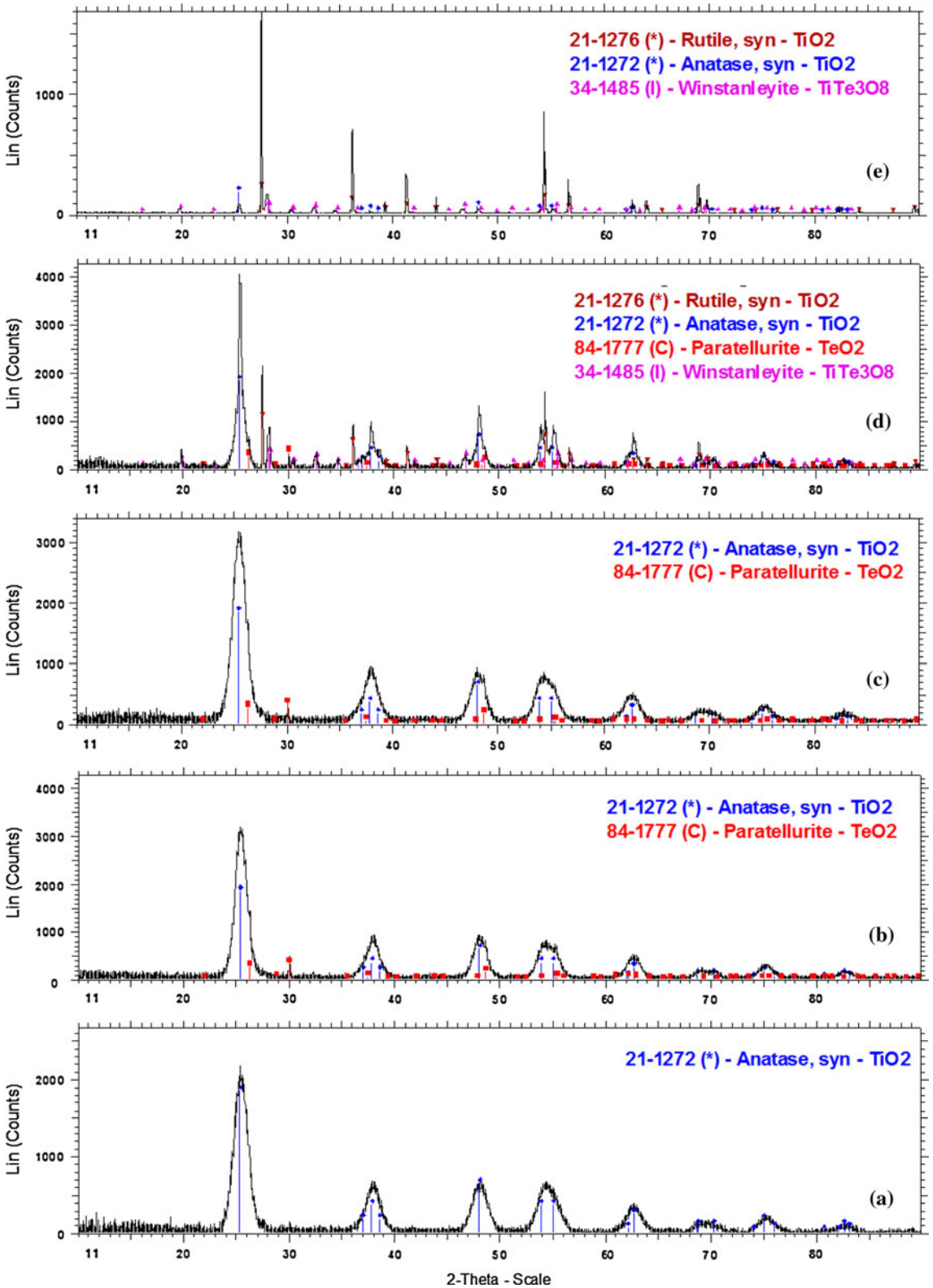

Fig. 3 XRD spectra of Te-doped titania heated at 400 °C. **a** TiTe1, **b** TiTe2, **c** TiTe3, **d** TiTe4, **e** TiTe5

photocatalysis but also for any physicochemical method [17]. Direct photolysis employing artificial UV light or solar energy source cannot mineralize Orange II [18]. Kinetics of the photocatalytic degradation of aqueous Orange II dye solution was measured by using a self-constructed photoreactor [19]. The photoreactor consists of a stainless steel cover and quartz tube with fluorescent lamp Narva with power 13 W and light intensity $\sim$3.5 mW cm^2. Black light (365 nm) for UV and warmwhite (upon 400 nm) for visible light irradiation were used. Orange II dye solution was circulated by means of membrane pump through flow cuvette. The concentration of Orange II dye was determined by measuring absorbance at 480 nm [20] with Vis spectrophotometer ColorQuestXE. The 0.5 g of titania sample was sonicated for 10 min with a ultrasonic bath (300 W, 35 kHz) before use. The pH of the resulting suspension was taken as the initial value for neutral conditions and under the experiment was kept at value 7.0.

Results and discussion

The XRD spectra of the Se-doped titania samples heated at 200 and 400 °C in oxygen atmosphere are presented in Fig. 1, the phase constitution and crystallite size are presented in Tables 2 and 3. All of the samples heated at 200 °C consist of anatase and amorphous Se phases, the samples heated at 400 °C consist only of anatase and no other phases can be found. The presence of the anatase phase was confirmed by comparing JCPDS standard files PDF 21-1272. A closer look at Fig. 1 indicates that the broadening of FWHM is observed with the increase in Se-doping with consequent increase in particle size. This is a reflection of modified TiO_2 properties with the addition of Se. A clear shift in the peak to the higher scattering

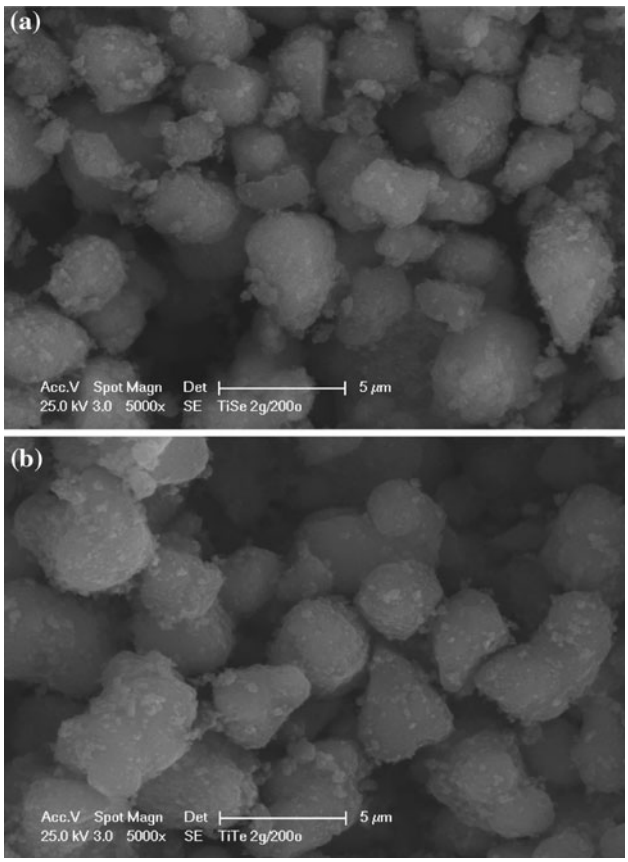

Fig. 4 SEM images of samples **a** TiSe2_200 and **b** TiTe2_200

Table 4 Phase composition and crystallite size of 400 °C heated samples TiO_2/Te

Sample	Anatase TiO_2 (wt%)	Rutile TiO_2 (wt%)	Paratellurite TeO_2 (wt%)	Winstanleyite $TiTe_3O_8$ (wt%)	Anatase TiO_2 (nm)	Rutile TiO_2 (nm)	Winstanleyite $TiTe_3O_8$ (nm)
TiTe1_400	100.00	0.00	0.00	0.00	15.5	–	–
TiTe2_400	99.48	0.30	0.22	0.00	15.3	–	–
TiTe3_400	98.76	0.99	0.24	0.00	14.2	77.3	–
TiTe4_400	79.71	16.11	0.00	4.18	29.8	270.0	54.4
TiTe5_400	5.50	90.05	0.00	4.45	71.8	396.0	85.5

Table 5 EDX, BET, and pore size distribution of 200 °C heated samples TiO_2/Se/Te

Sample	Surface area (m^2 g^{-1})	Total pore volume (cm^3 g^{-1})	EDX Se (wt%)	Sample	Surface area (m^2 g^{-1})	Total pore volume (cm^3 g^{-1})	EDX Te (wt%)
TiSe1_200	276.1	0.2173	3.14	TiTe1_200	292.8	0.2079	3.3
TiSe2_200	243.0	0.2173	5.73	TiTe2_200	306.9	0.2528	5.4
TiSe3_200	214.3	0.2972	11.52	TiTe3_200	269.6	0.2309	8.2
TiSe4_200	186.2	0.1730	16.07	TiTe4_200	225.2	0.1959	14.3
TiSe5_200	144.2	0.1255	18.24	TiTe5_200	201.7	0.1668	18.1

angle with the increase of particle size and with the increase of Se-doping was observed. The ionic radius of Se is 0.069 nm [21], and ionic radius of Ti is 0.0605 nm [22]. Selenium incorporation into TiO_2 corresponds to the change color to orange.

The XRD spectra of the Te-doped titania samples heated at 200 °C are in Fig. 2 and heated at 400 °C are presented in Fig. 3, the phase constitution and crystallite size are presented in Tables 3 and 4. All of the samples Te–TiO_2 heated at 200 °C consist of anatase and amorphous Te phases. More interesting are the samples calcined at 400 °C. The sample named TiTe_1 is formed only anatase phase, the sample TiTe_2 and TiTe_3 are anatase with traces ($\sim$0.2%) of TeO_2 (paratellurite, PDF 84-1777). Samples TiTe_4 and TiTe_5 consist of anatase, rutile and approximately of 4% $TiTe_3O_8$ (winstanleyite, PDF 34-1485). In the sample is already TiTe_5 dominant rutile phase (PDF 21-1276).The presence of rutile phase may occur due to a reduction in the photocatalytic activity.

The specific surface area of the samples, calculated by the multi-point Brunauer–Emmett–Teller (BET) method and total pore volume are listed in Tables 1, 2, and 5. With increasing content of Se and Te in both non-annealed samples and samples annealed at 200 °C, specific surface area decreases slightly. Conversely, in Se–TiO_2 doped samples heated to 400 °C is the trend reversed and the surface area grows with increasing the content of Se. For samples Te–TiO_2 heated at 400 °C with increasing of Te content the specific surface area rapidly decreased to a value of $\sim$4.5 $m^2\ g^{-1}$ for a sample denoted TiTe_5. This change of surface area is given an anatase to rutile transformation. According to IUPAC notation, microporous materials have pore diameters of less than 2 nm and macroporous materials have pore diameters of greater than 50 nm; the mesoporous category thus lies in the middle. For the all Se and Te-doped titania samples there is typical isotherm of a type IV isotherm characteristic of mesoporous material with type H2 hysteresis, which is a characteristic of mesoporous materials and can be ascribed to capillary condensation in mesopores. The size of mesopores is on the border with micropores, corresponding to size of 3–4 nm. According de Bore's characterization [23], all samples have characteristic of Type E hysteresis loop. This hysteresis type is connected with with ink-bootle pores or with interconnected capillaries.

The SEM images of samples labeled TiSe2_200 and TiTe2_200, respectively, are presented in Fig. 4. All Se and Te-doped titania powders consist of 1–2 μm spherical

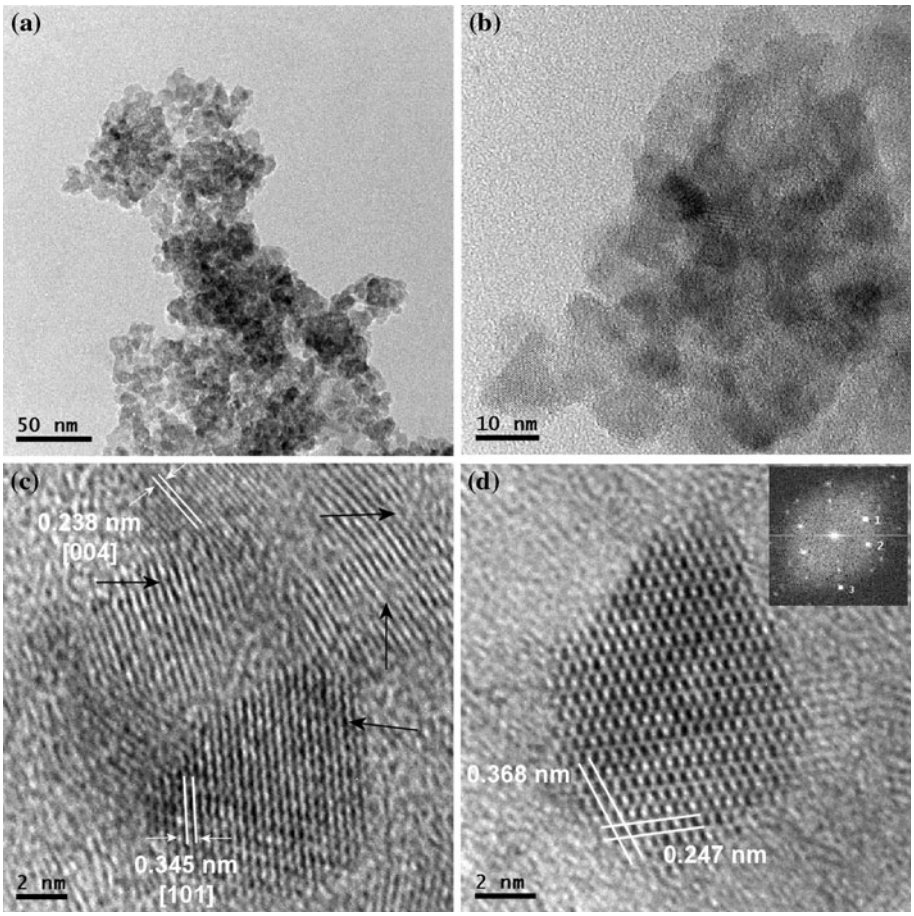

Fig. 5 HRTEM images of sample TiSe1_400: **a** magnification 60,000×, **b** magnification 250,000×, **c** magnification 1,200,000×, *arrows* indicate distortions and dislocations, **d** *inset* image of FFT pattern

clusters. Based on the HRTEM results (see Figs. 5, 6), these spherical particles consist of primary 4–5 nm anatase nanocrystals interlayed by small fraction of amorphous material.

The HRTEM images of the sample TiSe1_400 is presented in Fig. 5. The anatase (101) lattice spacing (0.345 nm) and (004) lattice spacing (0.238 nm) can be seen in Fig. 5c. These values are assigned to the (101) and (004) of anatase. The arrows in Fig. 5c indicate distortions [24] and dislocations [25] on anatase (101) face. These distortions and dislocations were probably attributed to electric stress, which may be originated from Se^{4+} ion doping. The high-resolution image (Fig. 5d) shows atomic planes with lattice spacings of 0.368 and 0.247 nm, respectively. Inset image of FFT pattern obtained from HRTEM, where spot 1 (101) and 2 (101) have d-spacing 0.368 nm and spot 3 (004) have d-spacing 0.247 nm. These values are expanded lattice caused by incorporation of Se atoms can be assigned to (101) and (004) atomic planes with lattice spacings of 0.352 and 0.237 nm (PDF 21-1272), respectively.

The HRTEM images of the sample TiTe1_400 is presented in Fig. 6. The expanded anatase (101) lattice spacing (0.368 nm) due to incorporation of Te^{4+} ions can be seen in Fig. 6c. This sample compared TiSe1_400 sample contains larger amount of amorphous domains (denoted with circle). The occurrence of these amorphous domains can influence a negative strong impact on photocatalytic activity [26]. The distortions and dislocations caused by the incorporation of Te^{4+} ions into the anatase lattice are shown in Fig. 6d.

Figures 7 and 8 present UV/Vis absorption spectra of the as-prepared samples Se and Te-doped titania samples heated at 200 and 400 °C, respectively. The prepared Se and Te-doped titania exhibit new optical properties concerning about the absorption, which are different from those of the titania. The reflectance data obtained was relative percentage reflectance to a non-absorbing material ($BaSO_4$) which can optically diffuse light. The Kubelka–Munk theory is generally used for the analysis of diffuse reflectance spectra obtained from weakly absorbing samples. It provides a correlation between reflectance and concentration. The concentration of an absorbing species can be determined using the Kubelka–Munk formula:

$$f(R) = (1 - R)^2/2R = k/s = Ac/s \quad (1)$$

where R is the reflectance, s is the scattering coefficient, k is the molar absorption coefficient, c is the concentration of the absorbing species, and A is absorbance [27].

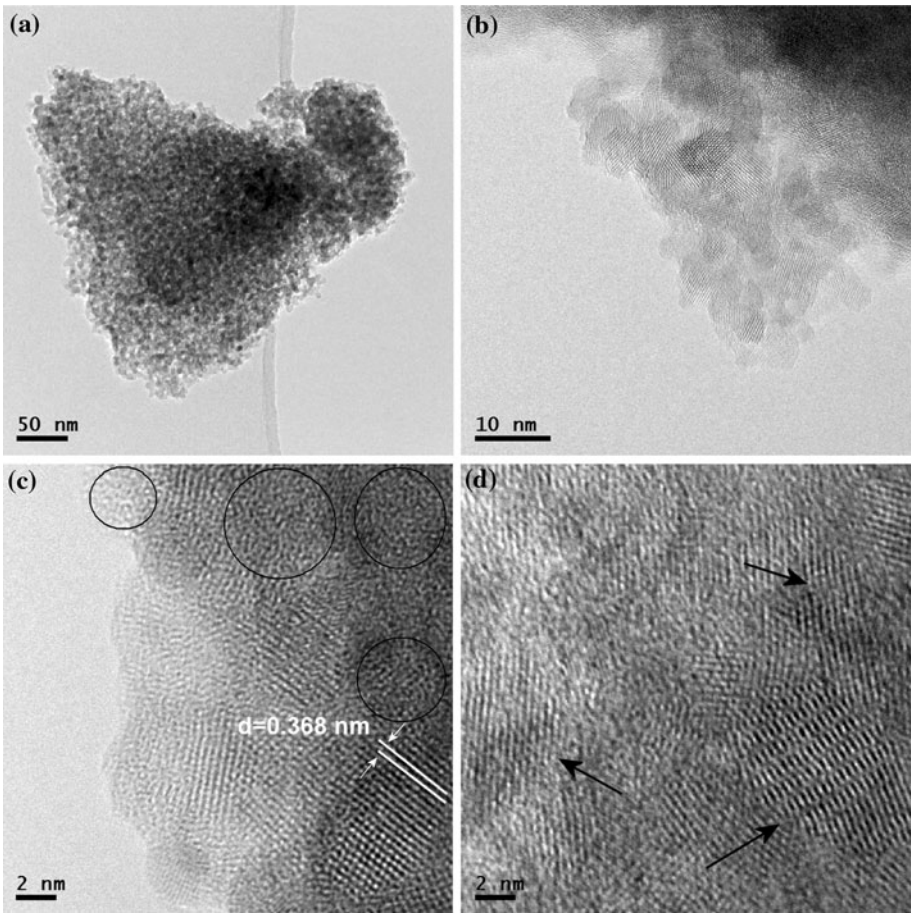

Fig. 6 HRTEM images of sample TiTe1_400: **a** magnification 40,000×, **b** magnification 300,000×, **c** magnification 1,200,000×, *circle* indicate amorphous domains, **d** *arrows* indicate distortions and dislocations

Compared with the pure TiO_2 sample, obvious absorption edge red shifts are observed in the results of the doped samples, among which the best response to visible light is obtained in the all doped sample.

The method of UV/Vis diffuse reflectance spectroscopy was employed to estimate band-gap energies of the prepared samples Se–TiO_2 and Te–TiO_2, respectively. Firstly, to establish the type of band-to-band transition in these synthesized particles, the absorption data were fitted to equations for direct band-gap transitions. The minimum wavelength required to promote an electron depends upon

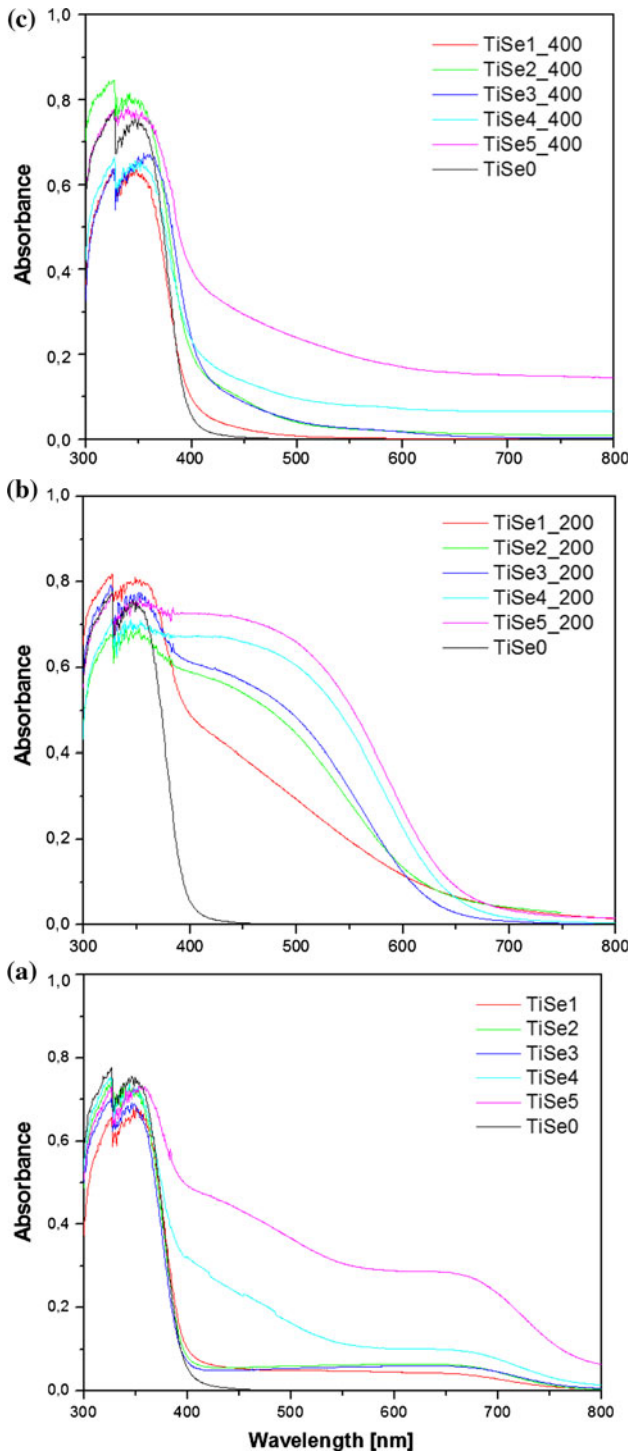

Fig. 7 UV–Vis diffuse reflectance spectra of samples **a** unheated TiSe, **b** heated TiSe at 200 °C, **c** heated TiSe at 400 °C

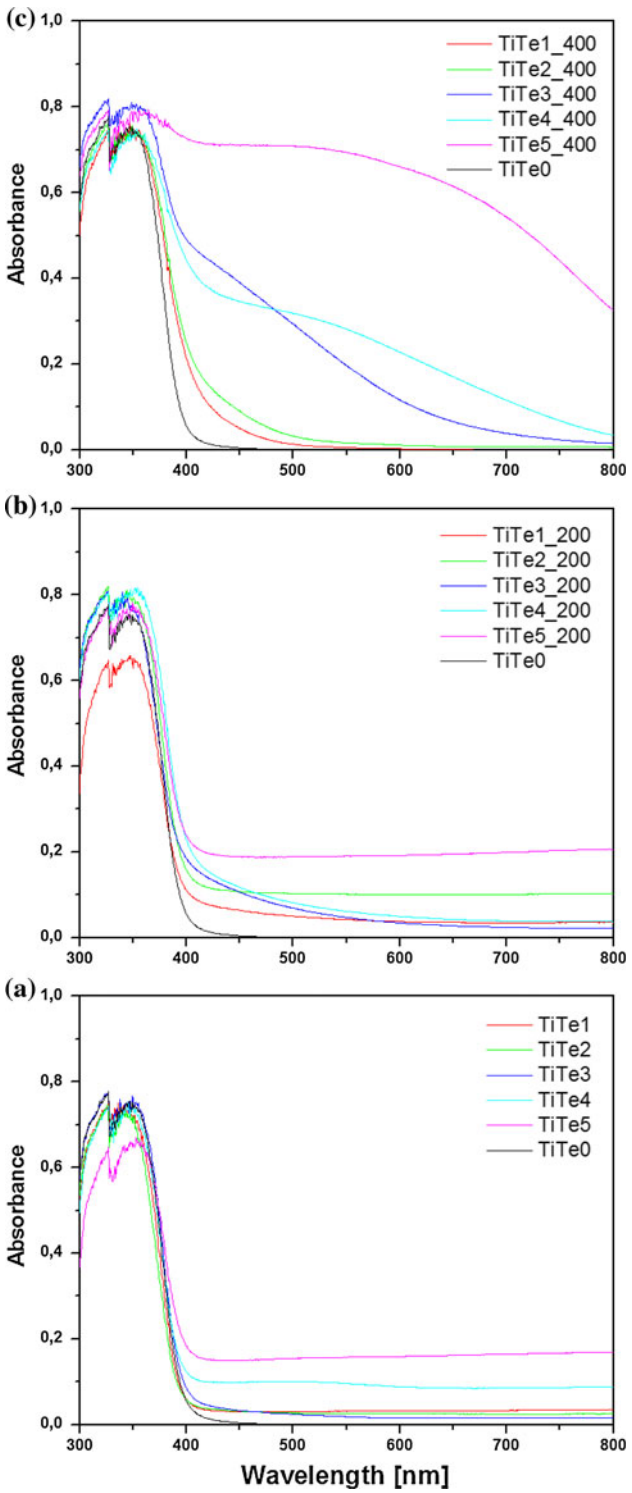

Fig. 8 UV–Vis diffuse reflectance spectra of samples **a** unheated TiTe, **b** heated TiTe at 200 °C, **c** heated TiTe at 400 °C

the band-gap energy E_{bg} of the photocatalyst and is given by:

$$E_{bg} = 1240/\lambda \text{ [eV]} \quad (2)$$

where λ is the wavelength in nanometers [28, 29].

The band-gap values were calculated using the UV–Vis spectra from the following equation:

$$\alpha(hv) = A\left(hv - -E_{bg}\right)^{m/2} \quad (3)$$

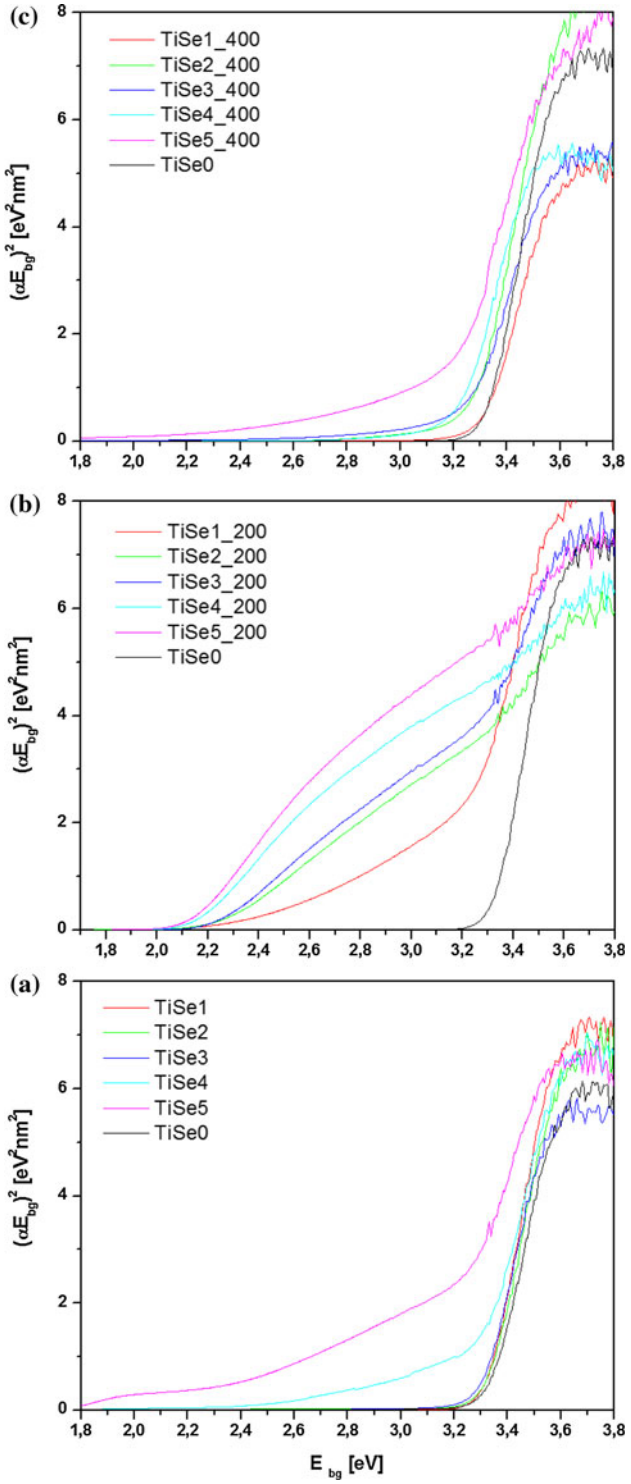

Fig. 9 Band-gap energy of samples **a** unheated TiSe, **b** heated TiSe at 200 °C, **c** heated TiSe at 400 °C

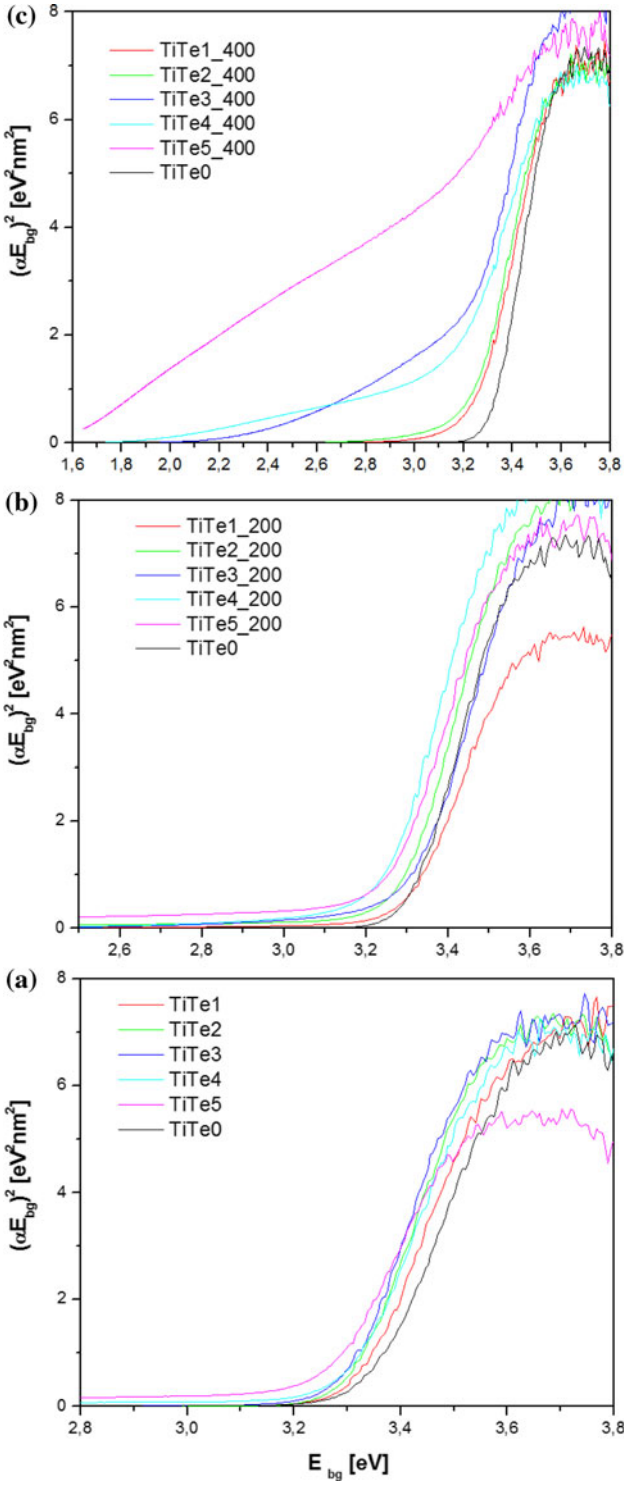

Fig. 10 Band-gap energy of samples **a** unheated TiTe, **b** heated TiTe at 200 °C, **c** heated TiTe at 400 °C

where α is the absorption coefficient, hv is the photon energy, and $m = 1$ for a indirect transition and $m = 0$ for direct transition [30], respectively, between bands and the energy of the band gap is calculated by extrapolating a straight line to the abscissa axis, when α is zero, then $E_{bg} = hv$ [31].

Figures 9 and 10 show the $(\alpha E_{bg})^2$ versus E_{bg} for a indirect band-gap transition, where α is the absorption coefficient and E_{bg} is the photon energy. The value of E_{bg} extrapolated to $a = 0$ gives an absorption energy, which corresponds to a band-gap energy (see Tables 6, 7, 8). The value of 3.20 eV for sample denoted as TiSe0/TiTe0 is reported in the literature for pure anatase nanoparticles [29]. The value of band-gap energy decreases with increasing content of Te and Se dopant. The elementary Se and Te can deposit onto TiO_2 lattice and shift the absorbance of the Se–TiO_2 composite to the visible region due to Se have narrow band gap 2.0 eV [32]. Tellurium is a narrow band gap p-type semiconductor with a band gap of $E_{bg} = 0.32$ eV [33].

Band-gap energy red-shift of the non-heated samples of Se-doped titania is due to elemental Se, which corresponds to light gray color of samples. Intense orange color of the samples annealed at 200 °C and the red-shift of the band-gap energy to a value given 2 eV is given to incorporation of Se into titania. The samples annealed at 400 °C have been not so intense color and value of the band-gap energy is not so low, which may be due to of partial sublimation ($\sim$315–317 °C) of selenium(IV) oxide in the annealing at temperature 400 °C (confirmed by the condensation of the sublimate in a cool part of quartz tube). Smaller band-gap energy of red-shift for samples TiO_2/Te and TiO_2/Te heated at 200 °C is given again amorphous tellurium, as in the case of the samples TiO_2/Se. The Te incorporation into TiO_2 causes intense yellow to brown coloration of the samples annealed at 400 °C and the red-shift of the band-gap energy to a value of 1.6 eV for the sample labeled TiTe5_600.

The photocatalytic activity of the prepared samples was determined using the degradation of 0.02 M Orange II dye

Table 6 Rate constant k and band gap of non-heated samples TiO_2/Se/Te

Sample	Band gap (eV)	k 365 nm (min^{-1})	k 400 nm (min^{-1})	Sample	Band gap (eV)	k 365 nm (min^{-1})	k 400 nm (min^{-1})
TiSe1	3.1	0.01479	0.00265	TiTe1	3.1	0.01048	0.00527
TiSe2	3.1	0.02402	0.00376	TiTe2	3.1	0.01181	0.00596
TiSe3	3.1	**0.03672**	**0.00907**	TiTe3	3.1	**0.02359**	**0.00673**
TiSe4	2.2	0.01229	0.00247	TiTe4	2.9	0.01395	0.00239
TiSe5	1.8	0.00958	0.00156	TiTe5	3.0	0.00719	0.00209

Table 7 Rate constant k and band gap of 200 °C heated samples TiO_2/Se/Te

Sample	Band gap (eV)	k 365 nm (min^{-1})	k 400 nm (min^{-1})	Sample	Band gap (eV)	k 365 nm (min^{-1})	k 400 nm (min^{-1})
TiSe1_200	2.2	0.00622	0.00321	TiTe1_200	3.0	0.01174	0.00228
TiSe2_200	2.1	0.01486	0.00422	TiTe2_200	2.9	0.01120	0.00370
TiSe3_200	2.1	**0.01837**	**0.00538**	TiTe3_200	2.8	**0.02267**	**0.00692**
TiSe4_200	2.0	0.01410	0.00441	TiTe4_200	2.7	0.01678	0.00437
TiSe5_200	2.0	0.00956	0.00440	TiTe5_200	2.6	0.00754	0.00178

Table 8 Rate constant k and band gap of 400 °C heated samples TiO_2/Se/Te

Sample	Band gap (eV)	k 365 nm (min^{-1})	k 400 nm (min^{-1})	Sample	Band gap (eV)	k 365 nm (min^{-1})	k 400 nm (min^{-1})
TiSe1_400	3.1	**0.00943**	0.00278	TiTe1_400	2.9	**0.00682**	0.00200
TiSe2_400	2.8	0.00474	0.00316	TiTe2_400	2.8	0.00645	0.00147
TiSe3_400	2.4	0.00234	**0.00533**	TiTe3_400	2.1	0.00662	**0.00241**
TiSe4_400	2.4	0.00221	0.00470	TiTe4_400	1.8	0.00267	0.00127
TiSe5_400	2.2	0.00174	0.00288	TiTe5_400	1.6	0.00134	0.00046

aqueous solutions under UV radiation at 365 nm (UV-A, black lamp) and up to 400 nm (warmwhite lamp). In regions in which the Lambert–Beer law is valid, the concentration of the Orange II dye is proportional to absorbance:

$$A = \varepsilon c l \tag{4}$$

where A is absorbance, c is concentration of absorbing component, l is length of absorbing layer, and ε is molar absorbing coefficient. Orange II dye has not a subject of photolysis and any change in Orange II dye concentration can be attributed only to the heterogeneous photocatalysis. Photodegradation experiments of Orange II dye by catalysts process exhibited first-order kinetics with respect to the concentration of the organic compound. The time dependence of Orange II dye decomposition can be described using Eq. 5 for a reaction following first-order kinetics:

$$\frac{dC}{dt} = k(C_0 - C) \tag{5}$$

where C is the concentration of Orange II dye, C_0 is the initial concentration of Orange II dye, and k is the rate constant. According to the degradation pathway proposed by Zhao et al. [34], the main byproducts formed by the ozonation of azo dye are organic acids, aldehydes, ketones, and carbon dioxide. Meanwhile, Demirev and Nenov [35] suggested that the eventual degradation products of azo dye in the ozonation system would be acetic, formic, and oxalic acids. The reaction pathway for the visible light-driven photocatalytic degradation of Orange II dye in aqueous TiO_2 suspensions is schematically shown in paper [36].

The calculated degradation rate constants k (min^{-1}) are shown in Tables 6, 7, and 8 and kinetics of degradation of Orange II dye at 365 nm (Black light) and 400 nm (Warmwhite) on samples TiSe, TiTe and heated samples at temperature 200 °C (TiSe_200 and TiTe_200) are illustrated in Figs. 11 and 12.

As has been stated above (see Figs. 7, 8), elemental selenium (and Te) which is deposited on TiO_2 shifted the absorbance of system to the visible light region. In addition, if Se is enlightened, on its surface are generated e^- and h^+ pairs, due to them Se could be used as photocatalyst to degrade of organics pollutants [37]. When is TiO_2/Se exposed to visible light, the titania and Se can forms a

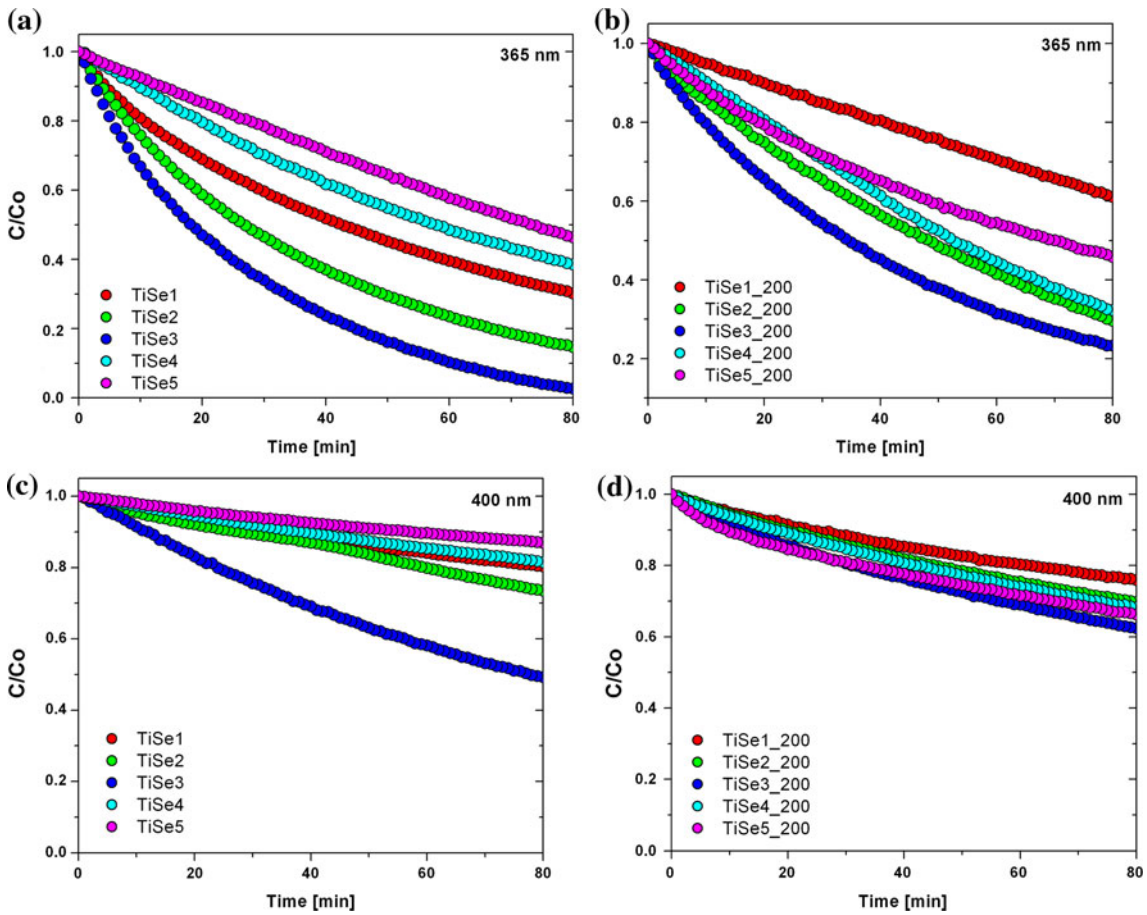

Fig. 11 Photocatalytic degradation Orange II dye at 365 nm of samples **a** unheated TiSe, **b** heated TiSe at 200 °C and at 400 nm, **c** unheated TiSe, **d** heated TiSe at 200 °C

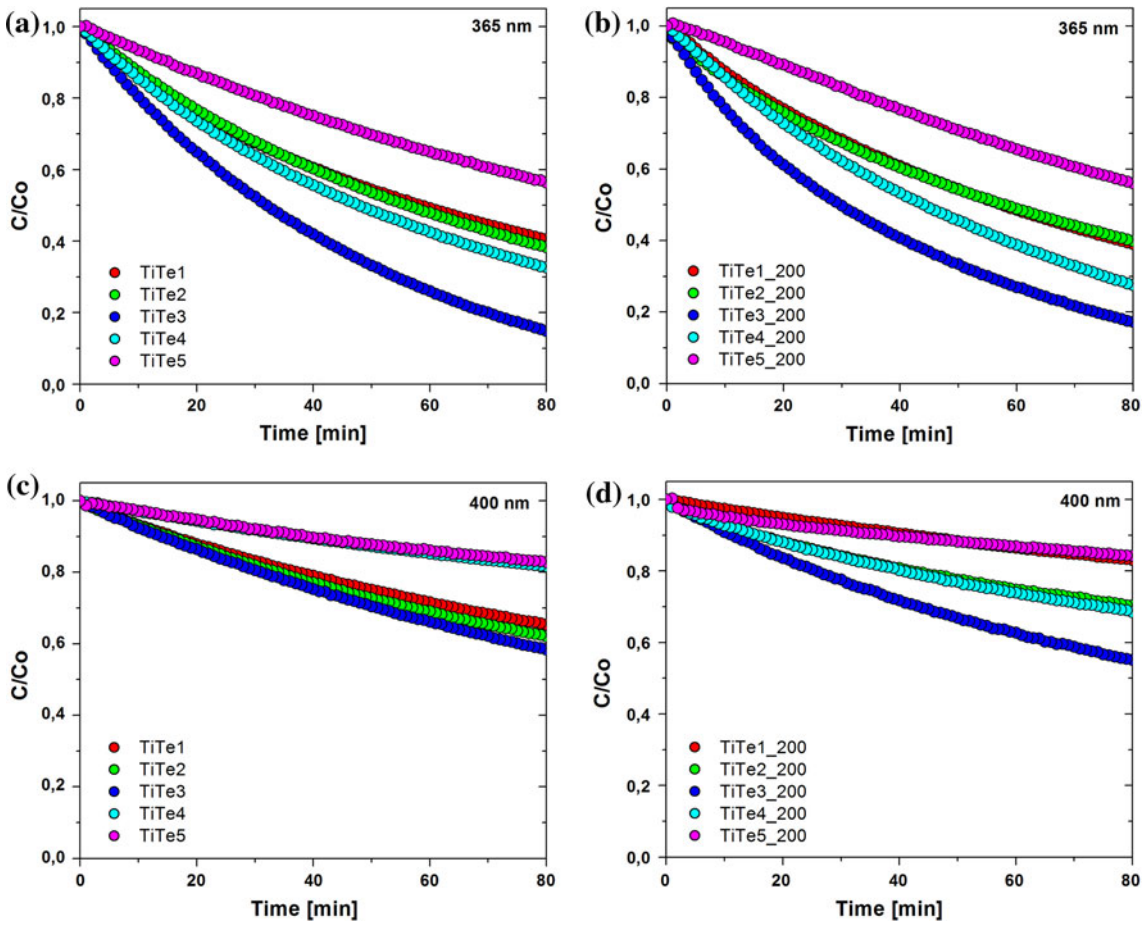

Fig. 12 Photocatalytic degradation Orange II dye at 365 nm of samples **a** unheated TiTe, **b** heated TiTe at 200 °C and at 400 nm, **c** unheated TiTe, **d** heated TiTe at 200 °C

n-TiO_2/p-Se "photochemical diode" in which the photocurrent is produced by transferring e^- from titania to Se [38]. This process may also prevent recombination of e^- and h^+.

The rate constant for undoped titania sample is $k = 0.00846\ min^{-1}$ in the UV region and $k = 0.00019\ min^{-1}$ for the visible light region. Se and Te doping increases the photocatalytic activity compared undoped titania for as-prepared samples and samples annealed at 200 °C in the UV region and for all samples in the visible region. Photocatalytic activity in the UV region decreases with annealing temperature. Decrease in photocatalytic activity may be due to loss of surface area. In the as-prepared samples and samples annealed at 200 °C exhibits the highest activity of samples labeled TiSe3 and TiTe3, respectively.

Lower photocatalytic activity of samples TiO_2/Te is given a greater presence of amorphous domains. For samples annealed at 400 °C have the highest activity samples labeled TiSe1_400 and TiTe1_400, containing according to XRD diffraction only anatase phase. Decreasing of photocatalytic activity in other samples annealed at 400 °C is mainly the origin of the rutile phase.

In the visible region of all samples are always the highest photocatalytic activity of samples labeled TiSe3 and TeTe3.

Conclusions

Titanium dioxide doped with different amounts of Se^{4+} and Te^{4+} ions, respectively, was prepared by homogeneous hydrolysis in the presence amorphous Se and Te. The prepared samples was annealed at temperature 200 and 400 °C. Te doping supports the transformation of anatase to rutile phase even at 400 °C, with increasing Te content increases the proportion of rutile phase. Incorporation of Se and Te into the anatase lattice have clearly positive effect on the photocatalytic activity in visible light area. The best photocatalytic activity in UV and visible area exhibit the Se^{4+} and Te^{4+}-doped titania samples labeled TiSe3 (~11.5 wt% Se) and TiTe3 (~8.0% Te), respectively. Using the above method of preparation that is easily transferable to industrial scale, can be prepared very low cost photocatalytic materials for UV and Visible region.

The same method is already produced TiO_2 for UV and visible region, where the Nd-doped TiO_2. Such prepared TiO_2 is the main ingredient is already manufactured photocatalytic self-cleaning paint for interior and exterior applications [39].

Acknowledgements This work was supported by the Academy of Sciences of the Czech Republic (Project No. AV OZ 40320502) and Czech Science Foundation (Project No. 203/08/0334).

References

1. Livraghi S, Paganini MC, Giamello E, Selloni A, Di Valentin C, Pacchioni G (2006) J Am Chem Soc 128:15666
2. Wang, Zhang Q, Yin S, Sato T, Saito F (2006) J Phys Chem Solids 68:189
3. Stengl V, Houskova V, Bakardjieva S, Murafa N (2010) Appl Mater Interfaces 2:575
4. Tojo T, Tachikawa M, Fujitsuka T, Majima J (2008) Phys Chem C 112:14948
5. Todorova N, Giannakopoulou T, Romanos G, Vaimakis T, Yu J, Trapalis C (2008) Int J Photoenergy 2008:1
6. Cui Y, Du H, Wen L (2008) J Mater Sci Technol 24:675
7. Hodgson SNB, Weng L (2002) J Mater Sci 37:3059
8. Phillips (2007) APS March meeting, American Physical Society, March 5–9, 2007
9. Wei W, Sheng-yi Z, Wen-zhi C, Yong-long Z, Yu-peng T (2008) Chem Res (1). doi:CNKI:SUN:HXYA.0.2008-01-002
10. Zhang S, Chen X, Tian Y, Jin B, Yang J (2007) J Cryst Growth 304:42
11. Nguyen VNH, Amal R, Beydoun D (2006) J Photochem Photobiol A: Chem 179:57
12. JCPDS PDF-2 release 2001, ICDD Newtown Square, PA, USA (2001)
13. ICSD Database FIZ Karlsruhe, Germany (2008)
14. Brunauer, Emmett PH, Teller E (1938) J Am Chem Soc 60:309
15. Barret EP, Joyner LG, Halenda PP (1951) J Am Chem Soc 73:373
16. Orel ZC, Gunde MK, Orel B (1997) Prog Org Coat 30:59
17. Lachheb H, Puzenat E, Houas A, Ksibi M, Elaloui E, Guillard C, Herrmann J (2002) Appl Catal B: Environ 39:75
18. Monteagudo JM, Durán A (2006) Chemosphere 65:1242
19. Stengl V, Housková V, Bakardjieva S, Murafa N, Havlin V (2008) Phys Chem C 112:19979
20. Bhattacharyya A, Kawi S, Ray MB (2004) Catal Today 98:431
21. Kunjomana AG, Chandrasekharan KA (2008) Cryst Res Technol 43(6):594
22. Pullar RC, Penn SJ, Wang X, Reaney IM, Alford NMcN (2009) J Eur Ceram Soc 29:419
23. De Boer JH (1958) In: Everett DH, Stone FS (eds) The structure and properties of porous materials. Butterworths, London, p 68
24. Liu F, Ding P, Yang X, Li J (2009) Nucl Instrum Method Phys Res B 267:3104
25. Liu ZL, Cui ZL, Zhang ZK (2005) Mater Charact 54:123
26. Colón G, Hidalgo MC, Navío JA, Pulido Melián E, González Díaz O, Doña JM (2008) Environmental 78:176
27. Christy AA, Kvalheim OM, Velapoldi RA (1995) Vib Spectrosc 9:19
28. Reddy KM, Manorama SV, Reddy AR (2002) Mater Chem Phys 78:239
29. Bhatkhande DS, Pangarkar VG, Beenackers AA (2001) J Chem Technol Biotechnol 77:102
30. Reyes-Coronado D, Rodríguez-Gattorno G, Espinosa-Pesqueira ME, Cab C, de Coss R, Oskam G (2008) Nanotechnology 19:1
31. Sanchez E, Lopez T (1995) Mater Lett 25:271
32. Chou, Yang S, Wang Y (2003) Mater Chem Phys 78:666
33. Chitralekha J, Gopal ESR, Chattopadhyay K (1997) J Mater Sci 32:2177. doi:10.1023/A:1018547510995
34. Zhao W, Shi W, Wang D (2004) Chemosphere 57:1189
35. Demirev A, Nenov V (2005) Sci Eng 27:475
36. Stylidi M, Kondarides DI, Verykios XE (2004) Appl Catal B 47(3):189
37. Nath S, Ghosh SK, Panigahi S, Thundat T, Pal T (2004) Langmuir 20:7880
38. de Tacconi NR, Chenthamarakshan CR, Rajeshwar K, Tacconi EJ (2005) J Phys Chem B 109:11953
39. http://www.detoxycolor.cz/english/index.htm